Cold Regions Science and Technology 69 (2011) 129–138

Contents lists available at ScienceDirect

Cold Regions Science and Technology

journal homepage: www.elsevier.com/locate/coldregions

Upward-looking ground-penetrating radar for measuring wet-snow properties

Christoph Mitterer [a,*], Achim Heilig [b,c], Jürg Schweizer [a], Olaf Eisen [c,d]

[a] WSL Institute for Snow and Avalanche Research SLF, Davos Dorf, Switzerland
[b] Commission for Glaciology, Bavarian Academy of Sciences and Humanities, Munich, Germany
[c] Institute of Environmental Physics, University of Heidelberg, Heidelberg, Germany
[d] Alfred Wegener Institute for Polar and Marine Research, Bremerhaven, Germany

ARTICLE INFO

Article history:
Received 9 January 2011
Accepted 8 June 2011

Keywords:
Wet-snow stratigraphy
Liquid water content
Impulse radar

ABSTRACT

Snow stratigraphy information is among other sources the key data for assessing avalanche danger—not only for dry snow but also for wet-snow conditions. Until now this information is obtained by traditional snow pit observations or more recently by applying more quantitative methods such as the snow micro-penetrometer or dielectric devices. All these methods are destructive and only provide a snap shot in time of snowpack evolution. We used an upward-looking ground-penetrating radar system (upGPR) to monitor snowpack evolution on a daily or, whenever necessary, hourly basis to obtain information on wet-snow properties. We focused on determining the volumetric liquid water content (θ_w) by calculating the effective permittivity (ε_{eff}) of the wet snow above the radar antennas, the advance of a wetting front and the wet-snow stratigraphy. ε_{eff} was obtained using the signal velocity and snow depth recorded with nearby ultrasonic gauges; θ_w was calculated with different mixing model approaches. Results were compared to in-situ measured permittivity, modelled wetting front advance and modelled and measured outflow at the bottom of the snowpack. The upGPR system clearly showed the advance of a wetting front and the arrival time was similar to the one recorded with a nearby lysimeter. Possibly weak wet layers with high liquid water content (θ_w>6%) were detected within the radar signal by multiple reflections. However, determining the exact amount of liquid water for each layer separately is still a task for future research.

1. Introduction

Assessing avalanche danger relies among other sources on information about snowpack layering and stability (e.g. McClung and Schaerer, 2006; Schweizer et al., 2003). In dry-snow conditions snow stratigraphy determines snowpack stability. Stability is assessed in the field by conventional snow pit observations usually combined with e.g. a structural instability index (Schweizer and Jamieson, 2007) or stability tests such as the Rutschblock test (Föhn, 1987). More recently, quantitative methods have been introduced including the snow micro-penetrometer (Bellaire et al., 2009; Schneebeli and Johnson, 1998) and near-infrared photography (Matzl and Schneebeli, 2006).

Despite advances, assessing wet-snow instabilities is still a difficult task and often prone to false-alarms (Mitterer et al., 2009). Air temperature is usually used as a proxy for predicting wet-snow avalanches (McClung and Schaerer, 2006) but often provides ambiguous results (Trautman, 2008). Nevertheless, air temperature is related to wet-snow avalanche activity (Baggi and Schweizer, 2009). Furthermore, it seems clear that the stratigraphy (Schneebeli, 1995), the isothermal state of the snowpack (Baggi and Schweizer, 2009; Techel and Pielmeier, 2010) and the advance of a wetting front (Mitterer et al., 2011) need to be considered for determining the size and timing of wet-snow avalanches. However, most statistically derived rules of thumb are valid only locally for a specific study region (Romig et al., 2005). A physical based approach is hindered by the fact that the wet snowpack is a porous medium with transient properties. Properties change in a highly non-linear manner and thereby the snow structure changes in a way that quantitative measurements become very complicated.

Bhutiyani (1994) related a considerable loss in shear strength to volumetric liquid water content values (θ_w)>6%. Observations and quantitative measurements at the crown fracture shortly after the release of a wet-snow avalanche showed that θ_w in the weak layer had reached values above 6% and running water was observed at the weak interface (Fierz and Föhn, 1995). Only few such quantitative observations exist. Mostly, θ_w is estimated using a wetness index (Fierz et al., 2009). However, properly estimating θ_w is very challenging even for experienced observers, and often these index-based values overestimate θ_w in comparison to actual measurements (e.g. Fierz and Föhn, 1995; Techel and Pielmeier, 2011). Several quantitative methods have been developed to determine the liquid water content in the field. These include cold (freezing) and hot (melting) calorimetry (Kawashima et al., 1998), alcohol calorimetry and the dilution method (Boyne and Fisk, 1990) as well as dielectric

* Corresponding author at: WSL Institute for Snow and Avalanche Research SLF, Flüelastrasse 11, CH-7260 Davos Dorf, Switzerland. Tel.: +41 814170216; fax: +41 814170110.
E-mail address: mitterer@slf.ch (C. Mitterer).

0165-232X/$ – see front matter © 2011 Elsevier B.V. All rights reserved.
doi:10.1016/j.coldregions.2011.06.003

measurements (e.g. Denoth et al., 1984). All these methods are destructive and provide only a short snap shot in time of wet snowpack evolution and thus stability.

Therefore, various studies focussed on using radar technology to record snowpack properties as electromagnetic waves enable non-destructive monitoring. Marshall and Koh (2008) reviewed the state of knowledge regarding the use of frequency modulated continuous wave (FMCW) radar systems for snow investigations. Besides FMCW radar technology, impulse radar systems such as e.g. commercial ground-penetrating radar systems (GPR) were applied to record snowpack properties as well. Roughly, for the past ten years, impulse radar systems were used to determine the snow water equivalent (SWE) (Lundberg et al., 1999; Lundberg and Thunehed, 2000; Marchand et al., 2001), to measure snow depth and its lateral variability (Harper and Bradford, 2003; Machguth et al., 2006) and to detect inhomogeneities, as e.g. buried avalanche victims (Heilig et al., 2008; Instanes et al., 2004; Modroo and Olhoeft, 2004).

Heilig et al. (2009) used an upward-looking GPR system (upGPR) and evaluated its feasibility for monitoring snow stratigraphy. They concluded that their system utilizing GPR antennas with a frequency of 900 MHz was able to detect significant changes in snow density and to even penetrate a moist snowpack. However, θ_w derived from the radar signal could not be validated as no additional measurements of θ_w were performed. They estimated only the wetness index (Fierz et al., 2009). The values of θ_w approximated by radar data analysis differed by at least 14% from the upper value of the range of liquid water content as indicated by Fierz et al. (2009) for the corresponding wetness index.

Within the presented work, we followed the preliminary findings of Heilig et al. (2009, 2010) in order to non-destructively monitor snowpack evolution. We installed a fully remote-controlled upGPR system beneath the snowpack (level to the soil surface) at Weissfluhjoch, Davos (Eastern Swiss Alps). We recorded snow parameters via upGPR on a daily and whenever necessary on an hourly basis, in particular during the melt season. The aim of the present study is to derive wet-snow properties, with special emphasis on monitoring the development of wetting fronts and determining the volumetric liquid water content of the snow above the radar antennas.

2. Methods

2.1. Data acquisition

In fall 2009 we buried an upward-looking ground-penetrating radar system (upGPR) in a wooden box at the Weissfluhjoch study site (2540 m a.s.l.) above Davos, Switzerland (Fig. 1). The top of the box was levelled with the soil surface. We used a commercially available GPR unit (RIS One GPR instrument, IDS, Pisa, Italy) with shielded 900 MHz antennas. The setup, operational procedure and processing sequence were comparable to the one presented by Heilig et al. (2010). The antennas were mounted on a hydraulic hoist system. The hoist was connected to a pump with an electric motor to allow vertical movement of the antennas. Utilizing remote-desktop software in combination with a permanent Internet connection and power supply, the radar system and the hydraulic lift were remotely controlled. One measurement set consisted of three single measurements. The highest uplift position of the antennas was about 1 cm below the top cover of the box, which is 1.5 cm thick.

In addition to the radar measurements, various instruments at the study site provided data on several other relevant parameters automatically. Those included θ_w measured with a 45° sloped SnowPower ribbon cable (Stähli et al., 2004), a 5 m^2 lysimeter for recording water outflow at the bottom of the snowpack and three ultrasonic

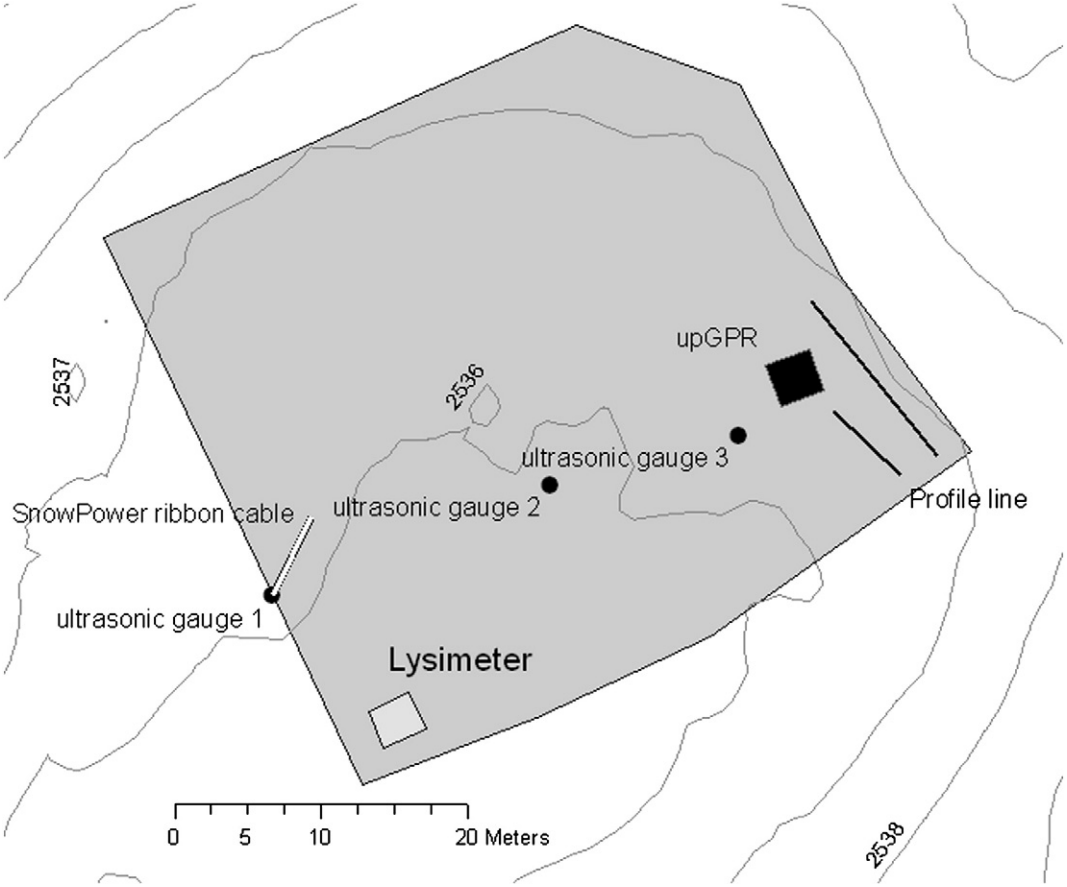

Fig. 1. Overview of the study site at Weissfluhjoch, 2540 m a.s.l., Davos, Switzerland. Black labels denote the position of the ultrasonic gauges, the upGPR system, the sloped ribbon cable and the lysimeter. The solid black lines show area where snow profiles where taken. Contour lines are in 1 m elevation increments.

gauges recording snow height at three different locations for the flat study site (Fig. 1). In addition, all required input parameters to run the 1-D snow cover model SNOWPACK (Bartelt and Lehning, 2002; Lehning et al., 2002a, b) are measured at the study site. Snow pit observations within a few meters (2–8 m) from the radar site were collected according to Fierz et al. (2009). In spring, θ_w was measured using a plate-type capacity probe (Denoth et al., 1984) with a vertical resolution of 5 cm. Snow density was determined layer-by-layer using a small (100 cm^3) cylinder and weighing it with an electronic scale. At least two measurements per layer were averaged.

2.2. Data processing

We applied a normalization function and the pre-processing filters as well as dewow and bandpass filters to the raw signal in a comparable way as published in Heilig et al. (2010). Differences in the processing steps resulted from the fact that the radar antennas were installed beneath the level of the soil surface and not in a snow cave above the soil. The surrounding coarse-grained and inhomogeneous soil influenced the signal and disturbing side reflections had to be removed. Therefore, we applied the linear gain not below a two-way travel time (TWT) of 4 ns and had to perform the background removal up to the position where the side reflections of the soil faded out (TWT ≅ 10 ns). The subsequent processing steps were again similar as described in Heilig et al. (2010). Utilizing a static correction the air gap between antennas and the top cover of the box was removed. Finally, as the reflection from the snow bottom was always recognizable in the data, it was possible to correct the start time of each profile to this media transition.

In addition to conventional radargrams, we display the signal information in compressed pulses as so-called p-wiggles (Fig. 2). This p-visualization was again performed in accordance with the approach discussed by Heilig et al. (2010). The only difference to their approach is that instead of employing only the first positive half cycle, we utilised the first positive half cycle and the subsequent, first negative half cycle and averaged both results for the display of the pulse compression. From these p-visualised wiggles we used the signal peaks of the first break to determine the TWT of specific reflections in the radargrams.

2.3. Dielectric permittivity

The relative effective dielectric bulk permittivity ε_{eff} above certain TWT-positions was calculated from the radar data according to e.g. Daniels (2004) with

$$\varepsilon_{eff} = \left(\frac{c}{v}\right)^2 \quad (1)$$

where $v = s/t$ is the wave speed in the penetrated medium (snow), c is the speed of light in vacuum, s is the height of specific layers or the whole snowpack and t is the travel time. To determine the total snow depth s we used the mean value of the two nearest ultrasonic snow depth gauges. For 24–25 April 2010, we assumed that below a TWT of 10 ns no changes occurred. The radar records support this assumption for these two days as below this TWT no modification in the radar records can be recognised (Fig. 2). For 28 April 2010, the height of the whole snowpack was used, as the percolation of water down to the bottom of the snowpack can no longer be excluded. We also assume that for wet snow Eq. (1) is applicable, as wet snow can still be considered a low-loss medium. In other words, the electrical conductivity values of wet snow are smaller than the product of circular frequency and permittivity. This assumption is justified by the fact that the values of θ_w were always far below 10% for the snowpack conditions analysed in this study and thereby the electrical conductivity of the whole snowpack is not influenced in a way that one has to consider it as an intermediate or high-loss medium.

Calculation of the volumetric water content θ_w is based on determining the relative effective bulk permittivity of a porous medium, in our case wet snow. The relative effective bulk permittivity ε_{eff} of a mixed non-magnetic media ($\mu_r = 1$) can be estimated either with an empirical relation (e.g. Topp et al., 1980) or a three phase mixing model (e.g. Perla, 1991; Roth et al., 1990):

$$\varepsilon_{eff} = \left[\theta_w \varepsilon_w^{\beta} + (1-n)\varepsilon_i^{\beta} + (n-\theta_w)\varepsilon_a^{\beta}\right]^{\frac{1}{\beta}} \quad (2)$$

where θ_w is the volume fraction of water, $\varepsilon_{i,a,w}$ are the dielectric properties for the three constituents, here ice (i), air (a) and water (w), β

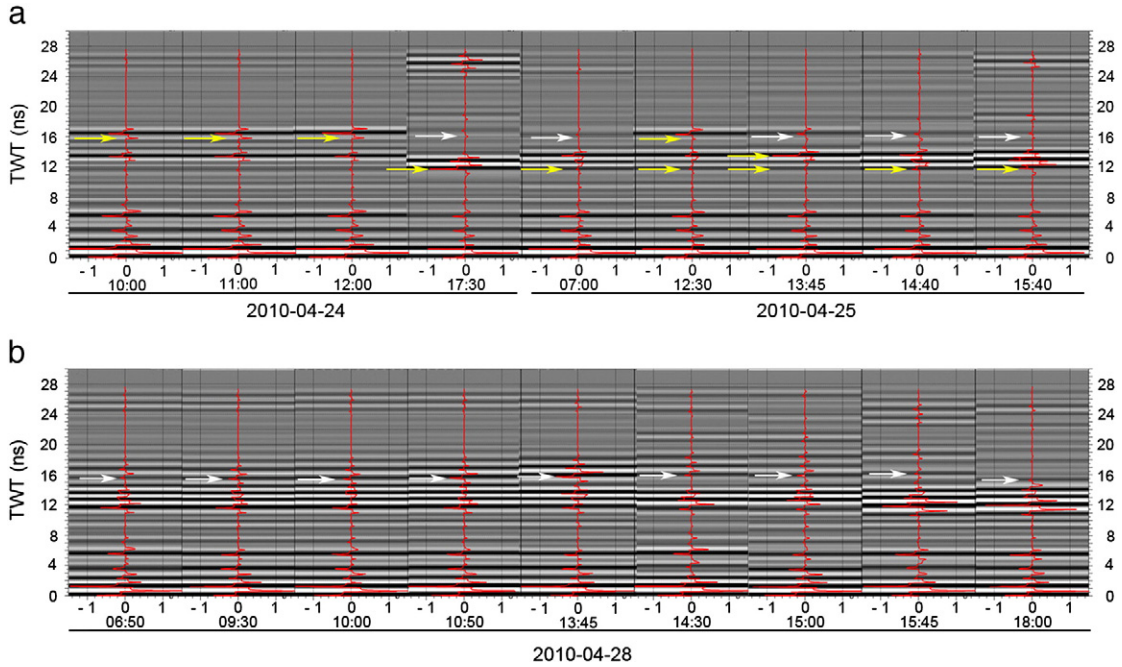

Fig. 2. Radargrams and p-wiggle for (a) 24–25 April 2010 and (b) 28 April 2010. White arrows indicate the snow surface, and yellow arrows show wetting front position. If only the yellow arrow is shown, the wetting coincides with the snow surface. If only the white arrow is shown, no clear wetting front could be determined.

is a factor considering the different layering of the investigated porous medium, and n is the porosity of snow defined as

$$n = 1 - \left(\frac{\rho_s}{\rho_i}\right), \tag{3}$$

with ρ_s and ρ_i the density of snow and ice, respectively. Inserting the value for the ε_{eff} obtained from the radar signals and the snow height values of the ultrasonic gauges, utilizing Eq. (1) in Eq. (2) and solving for θ_w yields

$$\theta_w = \frac{\varepsilon_{eff}^{\beta} - (1-n)\varepsilon_i^{\beta} - n\varepsilon_a^{\beta}}{\varepsilon_w^{\beta} - \varepsilon_a^{\beta}}. \tag{4}$$

Given that ε_w is frequency and temperature dependent, we assumed that $\varepsilon_w = 87.9$, $\varepsilon_i = 3.18$ and $\varepsilon_a = 1$. Roth et al. (1990) applied for β a value of -1 for a medium oriented vertically, 1 for a horizontal stratigraphy and 0.5 for a randomly oriented material. Many authors (e.g. Lundberg, 1997; Roth et al., 1990) found good agreement between calculated and measured ε_{eff} using the three phase mixing model and $\beta = 0.5$ for different porous media. However, Wilhelms (2005)also obtained good results while using $\beta = 1/3$ for wetted firn. In our study, we assumed $\beta = 0.5$ as, at the micro scale, wet snow can be considered as a random medium with no clear orientation.

Various formulations describing the three phase mixing models were presented in the past (e.g. Denoth, 1989, 1994; Lundberg and Thunehed, 2000; Sihvola and Tiuri, 1986). Denoth (1989, 1994) and Sihvola and Tiuri (1986) divided the influence of snow density ρ_s and volume fraction of water θ_w on ε_{eff} of wet snow according to

$$\varepsilon_{eff} = 1 + c_3\rho_s + c_4\rho_s^2 + c_5\theta_W + c_6\theta_W^2. \tag{5}$$

Based on Eqs. (2) and (5) Lundberg and Thunehed (2000) determined the constants as $c_3 = 1.7\times10^{-3}$, $c_4 = 7.244\times10^{-7}$, $c_5 = 15.06$ and $c_6 = 56.7$, calculated the average permittivity of wet snow and compared their results to measured one-way travel times of radar measurements obtained under laboratory conditions. When they changed c_5 to 23.7, they obtained a better fit, but the resulting value of $\varepsilon_w = 96.6$ indicates that using this value overestimates the permittivity of water.

Sihvola and Kong (1988) compared measurements to an empirical model using theoretically calculated relative dielectric permittivity values for wet snow and obtained the ε_{eff} with

$$\varepsilon_{eff} = 1 + 1.7\rho_s + 0.7\rho_s^2 + \left(0.1\theta_w\rho_w + 0.8(\theta_w\rho_w)^2\right)\varepsilon_w, \tag{6}$$

with the density of dry snow $\rho_d = \rho_s - \theta_w/\rho_w$. We used Eqs. (2)–(6) and calculated different values of θ_w assuming different theoretical values for ε_{eff} and an average snow density of $\rho_s = 340$ kg m^{-3}. The results are shown in Fig. 3. The theoretical relations for the formulations of Denoth (1989) and Roth et al. (1990) with $\beta = 0.5$ are almost identical. The values obtained with Eq. (6) follow a curve with a gentler slope than those obtained with Eqs. (2) and (5). Using the relation by Lundberg and Thunehed (2000), $\varepsilon_{eff} = 1$ corresponds to a θ_w of 0%, which is an inappropriate assumption as $\varepsilon_{eff} = 1$ is the permittivity of air. The value of $\varepsilon_{eff} \cong 1.5$ obtained with Eqs. (2), (5) and (6) agrees better with the permittivity of snow determined with a density of $\rho_s = 340$ kg m^{-3} and is in the range of seasonal dry-snow permittivity (Heilig et al., 2009). Therefore, we used Eqs. (2), (5) and (6) for calculating θ_w using the value of ε_{eff} obtained from the radar signal.

The reliability of ε_{eff} determined with the radar signal analysis depends on the accuracy and variability of the snow height measured with the ultrasonic gauges. Egli et al. (2009) estimated the variation of snow height measurements at the Weissfluhjoch study site to be in the range of 5% of the snow height. Fig. 4 shows the snow height obtained from the three ultrasonic gauges, the radar and the snow profiles. We excluded gauge 1 for further analysis, because (i) it measured almost all the time values above the mean of the three sensors, (ii) the sensor signal was very rough and contained many outliers, and (iii) the sensor was the farthest away from the radar location (Fig. 1).

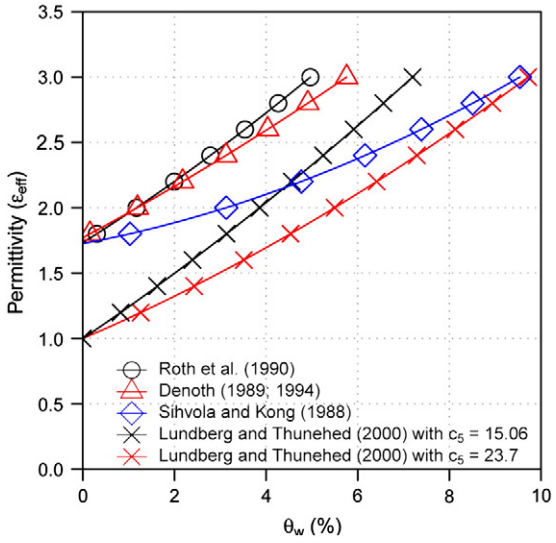

Fig. 3. Calculation of liquid water content (θ_w) for different theoretical values of effective permittivity ε_{eff} and density of snow $\rho_s = 340$ kg m^{-3} for the formulations introduced by Roth et al. (1990), Denoth (1989; 1994), Lundberg and Thunehed (2000) and Sihvola and Kong (1988).

As long as the snow was dry, the snow height calculated from the radar data showed good agreement with the mean value measured with the ultrasonic gauges (Fig. 4a). The coefficient of variation (COV) for the three ultrasonic gauges was on average below 5%. After including the snow height obtained from the radar into the calculation of the COV, the variation was still most of the time at about 5%, but increased as soon as parts of the snowpack became wet. Under wet-snow conditions, a constant mean wave speed can no longer be assumed and thus a simple conversion of TWT to snow depth is not applicable. To obtain a more reliable wave speed and thus calculate ε_{eff} we used the mean of gauges 2 and 3 with a range given by the values of gauges 2 and 3.

2.4. Modelling of wetting front

We compared the wetting front observed with the radar with two different modelling approaches using the snow cover model SNOWPACK. In addition, we used an analytical solution presented by Colbeck (1972) to obtain flux velocities at different heights of the snowpack.

The two different modelling approaches describe water flux within SNOWPACK using different water transport schemes. The mode I scheme uses a tipping-bucket threshold to transfer water from one snow element above the next element below. The threshold is fixed to water input, θ_w and snow density of one element. The second approach (mode II) uses the percolation theory of water in porous media proposed by van Genuchten (1980) and Mualem (1976). For both approaches, we assumed that whenever an element had a $\theta_w > 3\%$, water was draining downwards. The value of 3% was chosen as it is at the lower end of the values where the transition from the pendular to the funicular water regime is assumed to occur (Denoth, 1980). Above 3% water starts to be present in continuous patches, capillary forces will be reduced and gravity will determine the water flux. Both approaches are described in more detail by Hirashima et al. (2010) and Mitterer et al. (2011).

The calculation of water flux is based on the analytical solution for water percolation in firn presented by Colbeck (1972). We determined the velocity of water flux at any time step for each depth

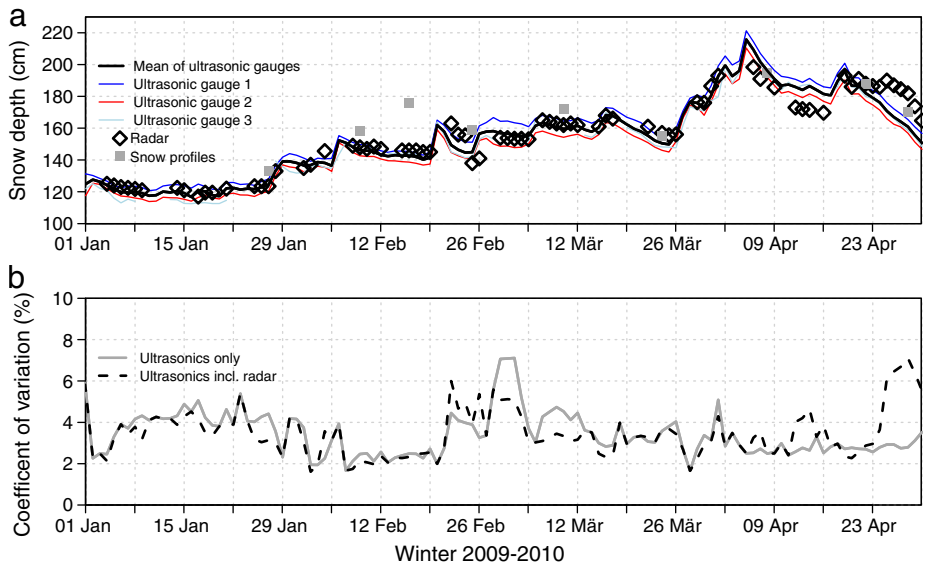

Fig. 4. Snow depth comparison of the ultrasonic gauges, the upGPR and depths in the snow profiles. (a) Blue, red and light blue lines show snow depth measured with gauges 1, 2 and 3, respectively. Black open diamonds indicate snow depth derived from radar measurements with a mean wave speed ($v = 0.23\ m\ s^{-1} \times 10^{-9}$); black line shows the average of the three ultrasonic gauges, grey squares show snow depth measured in the performed snow pits; (b) coefficient of variation of the three ultrasonic gauges (solid grey line) and of the three ultrasonic gauges including the radar values (dashed black line).

depending on snow density. The unknown input variables for solving the formulation are the input flux, the speed of propagation of the wetting front, and snow density. The input flux and speed of propagation were taken from the melting data modelled with SNOWPACK (see below) and the lysimeter data. The corresponding snow density was adopted from the snow pit measurements.

The water flux at the surface M_s was calculated from the energy balance:

$$M_s = \frac{1}{L}\left(\frac{dH}{dt} - \frac{d}{dt}\left(\rho_{ss} c_{p,i} T_{ss}\right)\right) \quad (7)$$

where dH/dt is the energy exchange at the snow surface, L the latent heat of fusion of ice ($3.34 \times 10^5\ J\ kg^{-1}$), $c_{p,i}$ the specific heat capacity of ice ($2.1 \times 10^3\ J\ kg^{-1}\ K^{-1}$); ρ_{ss} represents the density of the surface layer and T_{ss} is the snow surface temperature. For determination of the energy exchange, radiative fluxes were measured, whereas the turbulent fluxes were simulated with the bulk method (e.g. Arck and Scherer, 2002).

3. Results

We will shortly describe the snowpack evolution from the last week of March 2010 until the end of April 2010 and then report the results on the observed and modelled wetting front advance and the liquid water content.

The snowpack at the study site remained dry until the last week of March. The first wetting of the surface occurred around 21–23 March 2010. The snow pit profile obtained on 24 March 2010 revealed a wetted crust with a thickness of 5 cm. The profile was characterised by faceted crystals interrupted by several crusts. Until 16 April 2010 two snowfall events with rather cold temperatures altered with warmer periods, during which the surface was always wetted, but no penetration of percolating water to subsurface layers was observed or measured. Two dominant crusts developed and were consecutively covered with 10–20 cm of new snow. From mid April enhanced warming and solar radiation produced melt water. The profile taken on 22 April already revealed melt water percolation and several layers of refrozen water at capillary barriers down to a height of 138 cm (i.e. to a depth of ~50 cm), though the θ_w measurements indicated that no liquid water was present (Fig. 5) which was mainly due to the observation time (11:00 h). The breaking trough of melt water occurred between 24 April and 26 April 2010, as the lysimeter indicated first considerable outflow volumes for this period.

Fig. 2 displays the radargrams and p-wiggles (red line) of the reflected wave signal for the measurements performed on 24–25 April and 28 April. White arrows mark the snow surface; yellow arrows indicate the wetting front. During the morning measurements, the wetting was close to the snow surface (~16 ns). At the last observation, the wetting front had moved downwards to a TWT = 11 ns (corresponding to about 138 cm). In the snow pit performed two days before, a 5 cm thick crust was observed at 138 cm, which used to be the former surface at the first shallow wetting (21–23 March). Strong primary reflections and related multiples corresponding to that snow height, suggest that liquid water content was high above the crust. In-situ measurements, which were performed four days later, confirmed the ponding of water above the crust (Fig. 5b). On the following day, the wetting front was still at the same position, but beginning from 12:30 h a second wetting front started from the snow surface and reached the crust at 138 cm at 14:40 h (TWT = 11 ns). Again, the last radar measurement on that day indicated high liquid water content above the crust, with the same pattern of multiple reflections. The radargrams of 28 April (Fig. 2b) showed no clear wetting front advance; the snow surface was still visible, but harder to detect in the signal than for the previous days. Still, strong reflections were observed at 138 cm, but the multiple reflections were less pronounced. At 14:30 h the signal at about 5–6 ns showed a stronger peak in the p-wiggle than before, therefore, we assume that water drained from now on down to an old crust, which had developed in early winter. Full wetting of the snowpack probably occurred in the next days.

Fig. 6a compares the modelled wetting fronts to the ones observed with the radar; Fig. 6b shows the calculated melt water flux at the snow surface and the outflow recorded and modelled (mode II) at the bottom of the snowpack. Lysimeter outflow indicated that the wetting front arrived at the bottom of the snowpack in the afternoon of 24 April 2010; peak discharge was observed on 25 April and then again on 29 April. Wet-snow avalanche activity peaked on 25 April with several mixed and wet-snow avalanches reported in the surroundings of the Weissfluhjoch. No profiles were performed at fracture lines. Observations, however, suggest that the avalanches fractured slightly above the ground or at the snow–soil interface.

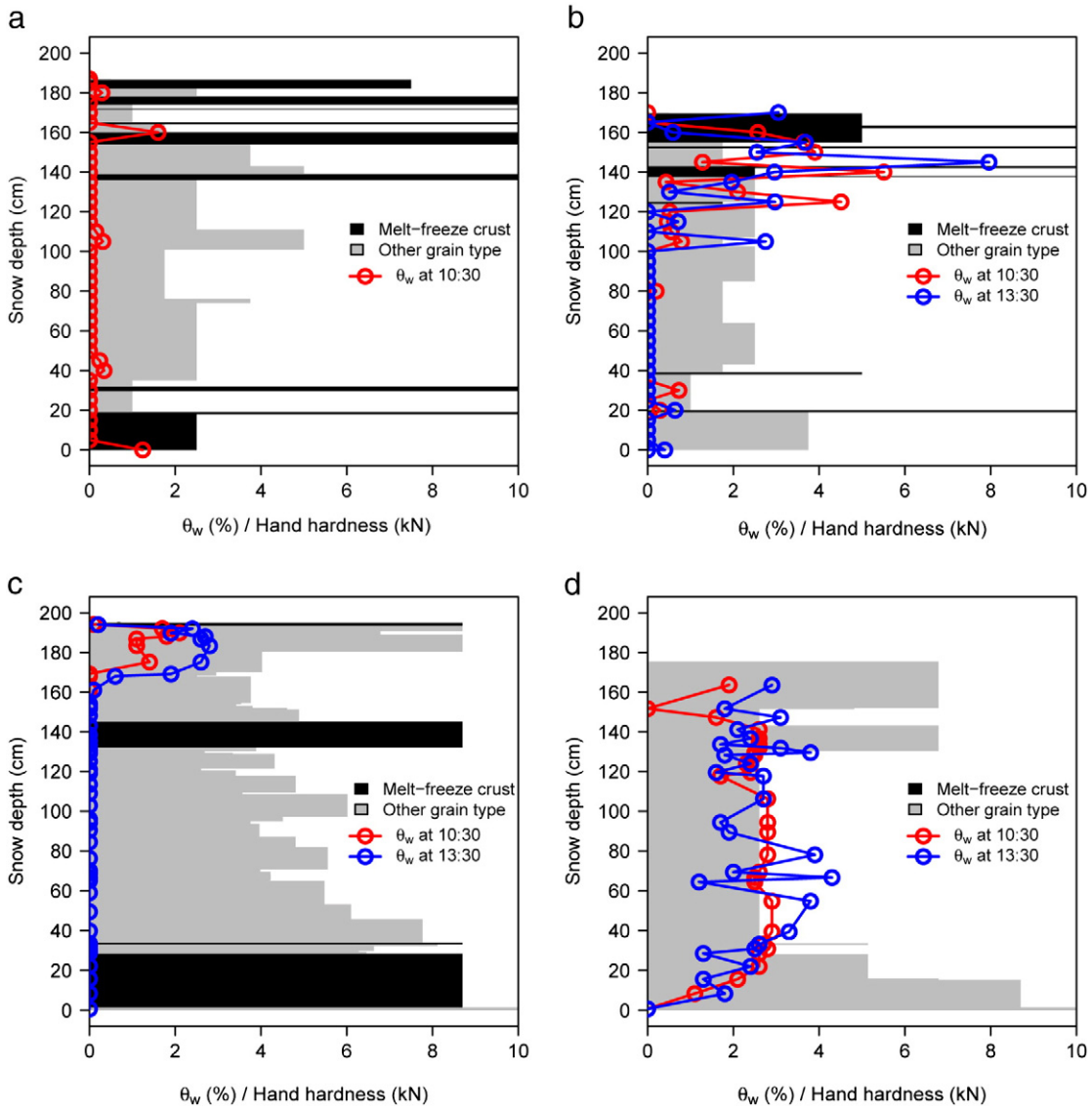

Fig. 5. Hand hardness, melt-freeze crust distribution and volumetric liquid water content (θ_w) measured with an in-situ capacity plate for (a) 22 April 2010 and (b) 28 April 2010; (c) and (d) show the simulated hand hardness, melt-freeze crusts and θ_w using SNOWPACK in mode II.

The results of the modelled wetting advance are comparable to those presented by Mitterer et al. (2011) and showed again a large difference between the two modes in arrival time at the bottom of the snowpack. The mode II water transport scheme predicted the arrival time of percolating water four days after the first considerable amount of water was recorded by the lysimeter and while the peak of wet-snow avalanche activity happened. The modelled outflow (Fig. 6b) is also in delay by four days and somewhat underestimates the fluxes with the exceptions of peak flux values at noon. Comparing the radar-recorded wetting to the modelled one in mode II reveals that the modelled advance is slightly too fast at the beginning, which is probably due to the parameterisation on which mode II is based (Yamaguchi et al., 2010). Ponding on the crust at 138 cm was captured, but ponding time was somewhat underestimated (Figs. 5d and 6a). Secondary wetting fronts were not modelled with either simulation approach. In mode I, the wetting front penetrated the whole snowpack not before mid May.

Only the data of 24 April 2010 were suited for the analytical solution by Colbeck (1972) (Fig. 6b). On the following days the peaks of the input flux at the surface was too low compared to the outflow measured with the lysimeter. Also the time delay between the two peaks was very short suggesting that the flow was either very fast or horizontally diverted water was routed into the lysimeter (Fig. 6b). However, on 24 April the area below the two curves was different as well. In other words, the lysimeter did not record the same amount of water, which was produced at the surface. The calculated mean flux velocity for 24 April was $V_m = 1.78 \pm 0.08 \times 10^{-3}$ cm s^{-1} according to the formulations of Colbeck (1972). Assuming a constant mean velocity, the water should arrive after 29 h at the bottom of the snowpack. Compared to Fig. 6b, this value appears to be very high as the peak influx at the surface arrived at the bottom of the snowpack only 7 h later. The discrepancy is due to the fact that for the calculation only data for one day were used. We neglected the influx, modelled for the previous days and thus, underestimated the real influx. Using the formulation of Colbeck (1972), however, revealed that the water flux decreased towards the position within the snowpack where the melt-freeze crust caused the ponding. This is in good agreement with the results derived from the radar signals and manual snow pit observations.

Table 1 shows ε_{eff} derived from the radar and the corresponding values of θ_w using either Eqs. (4) and (5), or (6) for the days of 24–25 April and 28 April. The values represent the average θ_w for the wet parts on 24–25 April and the entire snowpack for 28 April. These

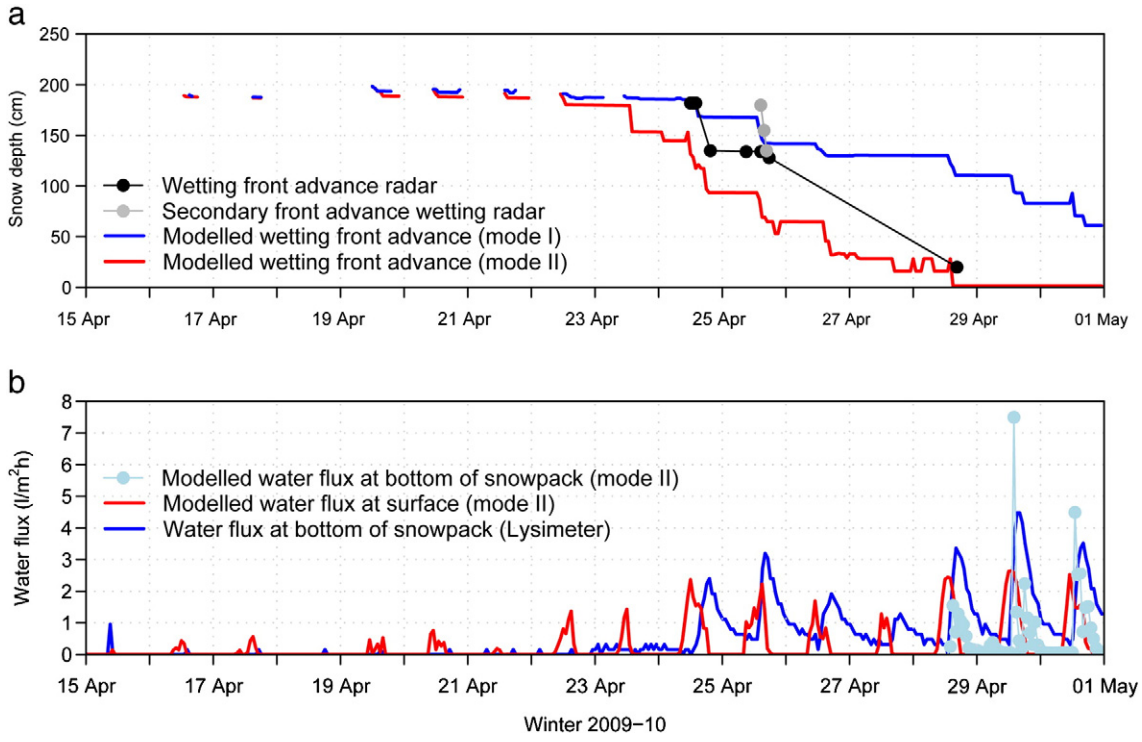

Fig. 6. (a) Modelled and measured wetting fronts for the study site Weissfluhjoch (2540 m a.s.l); (b) melt water flux at the snow surface (red) modelled with SNOWPACK and melt water flux at the bottom of the snowpack (blue) recorded with a 5 m^2 lysimeter and modelled with SNOWPACK in mode II (light blue).

values can be compared to the measurements we made with the capacity plate on 22 April and 28 April. The capacity plate measurements yielded values of $\theta_w = 0.9\%$ on 22 April and $\theta_w = 1.6\%$ on 28 April, just considering the wet parts of the snowpack (Fig. 5). If for 28 April we consider the entire snowpack, the value drops to 0.9%, whereas the value derived from the radar measurements was at least about 3%. When converted to mass of liquid water, 14 kg m^{-2} was obtained with the capacity probe, whereas an average of 29_54 resulted from the radar data (Fig. 7). The large variation is due to the different formulations for ε_{eff}. In particular, utilizing the formulation of Sihvola and Kong (1988) leads to the large values (Fig. 3). The SnowPower measurements yielded very high values for the volumetric fraction of water and clearly overestimated the real water content. As the sensor cable is sloped from a mast through the complete snow cover, it is likely that melt water drains along the cable into the snowpack and influences the measurements (Stähli et al., 2004).

In addition, the mass of water above the antennas was simulated with the snow cover model SNOWPACK (Fig. 7). Results were in good agreement with the values of the radar data analysis suggesting that the capacity probe rather underestimates the mass of liquid water.

Table 1
Relative effective bulk permittivity ε_{eff} calculated from the radar signals and corresponding volumetric liquid water content θ_w using either the formulation of Roth et al. (1990) (θ_R), Denoth (1989, 1994) (θ_D), and Sihvola and Kong (1988) (θ_S). Also shown are the mean (θ_{mean}) of the three θ_w values including the standard deviation, and the SnowPower ribbon cable (Stähli et al., 2004) (θ_{SP}). On 24–25 April 2010 θ_w is calculated for the top 50 cm of the snowpack (to a snow depth of 138 cm corresponding to a TWT = 10 ns); for 28 April the data represent an average over the complete snow depth. Only θ_{SP} is always calculated for the entire snowpack.

Date	Time	ε_{eff}	θ_R	θ_D	θ_S	θ_{mean}	θ_{SP}
24 Apr	10:00	1.77 ± 0	0.50	0.38	0.72	0.54 ± 0.17	4.7
	11:00	1.77 ± 0	0.69	0.60	1.25	0.85 ± 0.35	4.8
	12:00	1.84 ± 0	0.76	0.68	1.44	0.96 ± 0.41	4.8
	17:30	2.15 ± 0.06	1.63	1.71	3.45	2.26 ± 1.03	4.9
25 Apr	07:00	1.97 ± 0.03	1.17	1.16	2.43	1.6 ± 0.73	5.3
	12:30	1.99 ± 0	1.40	1.43	2.95	1.93 ± 0.9	5.0
	13:45	2.13 ± 0.03	1.74	1.83	3.67	2.41 ± 1.09	4.9
	14:40	2.09 ± 0.03	1.73	1.82	3.66	2.4 ± 1.09	5.1
	15:40	2.29 ± 0.03	2.55	2.80	5.23	3.53 ± 1.48	5.2
28 Apr	07:00	2.15 ± 0	2.12	1.55	4.90	2.86 ± 1.8	5.0
	09:30	2.16 ± 0	2.16	1.55	4.98	2.91 ± 1.8	5.4
	10:00	2.19 ± 0	2.27	1.6	5.18	3.06 ± 1.8	5.0
	10:50	2.17 ± 0.01	2.21	1.74	5.18	2.98 ± 1.8	5.0
	13:48	2.24 ± 0.03	2.49	2.00	5.56	3.35 ± 1.9	5.5
	14:30	2.31 ± 0.04	2.75	2.32	6.01	3.69 ± 2.0	5.4
	14:50	2.31 ± 0.06	2.74	2.31	5.99	3.68 ± 2.0	5.2
	15:45	2.39 ± 0.05	3.06	2.7	6.52	4.1 ± 2.1	5.3
	18:00	2.18 ± 0.05	2.25	1.71	5.14	2.11 ± 1.8	5.3

4. Discussion

The upGPR system was capable of detecting layer boundaries with changing liquid water content, tracking the advance of a wetting front and determining the amount of water for the entire snowpack and parts of it. However, differences in θ_w in a high vertical resolution (~2 cm) which are due to subtle changes in stratigraphy, can only be recorded utilizing the dielectric capacity plate (Fig. 5a, b). The radar, however, can detect layers with different liquid water contents when the water gradient among the layers is adequately pronounced and horizontally continuous; furthermore, the radar signal must not be obscured by other sources of signal scattering. Otherwise important information about a potential wet weak layer might be missed. While horizontal features like the ponding of liquid water above an impermeable layer can be clearly recorded by the radar signals (Fig. 2), capturing the size and horizontal distribution of vertical flow patterns (flow fingers) is very likely not possible with stationary upGPRs. Nevertheless, flow fingers can route significant amounts of water into deeper laying parts of the snowpack or to the ground (Waldner et al., 2004). The arrival of considerable amounts of water was recorded by the lysimeter two to three days before the radar indicated a percolation of water through the whole snowpack above the antennas. The delay might be due to various reasons: (i) variable flow patterns above the two devices—water flow may well be spatially variable (Machado, 2000; Techel and Pielmeier, 2011); (ii) the water transport for these days was mainly dominated by

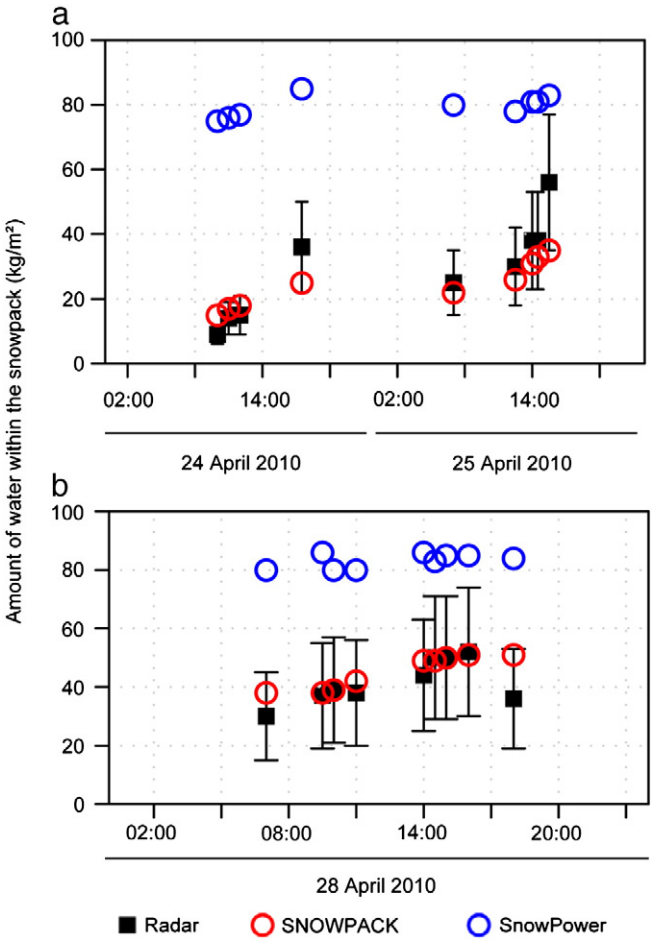

Fig. 7. Amount of liquid water above the radar antennas (mean θ_w for complete snowpack) derived from the radar signals (black square), calculated with the snow cover model SNOWPACK (red open dot), and measured with the SnowPower (blue open dot) ribbon cable for three days in April 2010. Black square shows the mean when using formulations of Eqs. (2), (5) and (6). Whisker shows the minimum and maximum obtained with the different formulations.

preferential flow paths; and (iii) the upGPR did not capture the percolation above the antennas. The last explanation appears to be rather unlikely as the amounts of water measured by the lysimeter lead to the assumption that percolation above the antennas would alter the signal response from the snowpack remarkably.

This study shows that the radar system is capable of monitoring layers with a temporarily high θ_w, e.g. above a melt-freeze crust. In our case, the occurrence of strong multiple reflections hints towards an increase of liquid water content above a crust. Further analyses are required to relate multiple reflections to the amount of θ_w. Signal attenuation, changes in propagation velocity of the radar signal and the appearance and disappearance of strong multiples are information, which may help to calculate θ_w for single layers or vertical traces. The propagating radar signal follows a frequency-dependent absorption and its relation to bulk θ_w was already reported in other GPR studies (e.g. Bradford et al., 2009). This signature might be useful for detecting wet weak layers automatically. More data have to be collected to be able to analyse these features. Changes within the signal will be very small and therefore an increase in resolution (space and time) will be needed for the approach suggested above.

The advances of the wetting front recorded with the upGPR are in good agreement with the modelled flow with SNOWPACK in mode II. This suggests that the radar captures mostly matrix flow behaviour as the mode II water transport scheme is based on matrix flow theory only and does not include preferential flow. It is astonishing that only matrix flow can produce such a fast downward routing and we believe that the true percolation behaviour is somewhere between the two modes. The discrepancy between the lysimeter data and the modelled and recorded fluxes and advances, respectively, might hint to periods with enhanced preferential flow activity. Water draining into the lysimeter recorded before the time expected based on the radar signals or the model originates either from flow fingers or horizontally diverted water. The existence of preferential flow and the fraction of water moving in flow fingers is, however, very difficult to estimate. The amount of water recorded with the lysimeter exceeds the amounts transported in flow fingers reported in previous studies. Albert et al. (1999) concluded that typically 3–4 flow fingers per square meter might transport 0.4 l h^{-1} m^{-2} and finger. Compared to our lysimeter recordings these estimates are exceeded by a factor of 3. Of course, different stratigraphy with many very porous snow layers might lead to higher fluxes, but also the discrepancy between the available water as modelled and the amount recorded with the lysimeter shows that horizontally distorted water must have dripped into the lysimeter. Subdividing the lysimeter might help to detect those irregular flow patterns.

The amount of water calculated with SNOWPACK in mode II agreed well with the amount estimated from the upGPR signal showing that SNOWPACK simulated the total amount of water about right, but cannot—for obvious reasons—reproduce the complex patterns of water flow in snow.

A device such as the impedance sensor SnowPower is able to describe the general trend when the liquid water content is increasing, but overestimates the total values, which is mainly due to the setup of the sensor. The sensor itself is sloped through the whole snowpack. Melting snow or rain will run along the cable sensor and will influence the measurement around the cable. Wind affects the position of the cable and produces potholes which again ease the infiltration of water but also disturb the coupling of the sensor with the surrounding snow matrix.

The discrepancy between the radar and the capacity device used in the snow profiles may be explained by the fact that the measurements with the capacity probe are performed at an open pit wall. It is very likely that water will drain as soon as the pit is excavated. The drainage can occur quite fast (Techel and Pielmeier, 2011) and values measured with the plate sensor may thus be too low. In addition, the water flux is likely to be highly variable at the scale of the snow pit (Techel and Pielmeier, 2011). Point measurements with the capacity probe might also be related to issues such as support volume and sampling design. The radar as a non-destructive measurement device has clear advantages in this respect.

5. Conclusions

We used an upward-looking ground-penetrating radar system (upGPR) to observe and quantify wet-snow properties. The chosen frequency of 900 MHz allowed for penetration of the complete snowpack of 1–2 m height, even though some layers had volumetric liquid water contents of 6–8%.

With two additional ultrasonic snow depth sensors we determined the effective permittivity ε_{eff} and calculated the liquid water content θ_w above the radar antennas using different mixing formulas.

The radar was capable of tracking the advance of wetting fronts. Differences in arrival time of the wetting front at the bottom of the snowpack between radar, lysimeter and simulation with SNOWPACK suggest that no conclusions can be made on the type of water flow. It is not clear how much flow fingers or capillary barriers affect the advance of percolating water especially in the early stage of complete wetting. Nevertheless, we have shown that the radar system can monitor layers with high θ_w, e.g. above a melt-freeze crust. In our case increasing multiple reflections hint towards an increase of θ_w above a crust. Further analyses with special regard on the frequency content, absorption and propagation

velocity within those multiple reflections are needed to interpret such signal features caused by layers of high θ_w. This signature might be useful for detecting wet weak layers automatically.

Comparison to modelled melt water amounts using the 1-D snow cover model SNOWPACK revealed that the amount of liquid water was similar suggesting that the melt water input calculated by SNOWPACK is about right, but the water flux is not implemented correctly. A 1-D model such as SNOWPACK might be too limited to adequately represent water flux behaviour in snow. In the future, radar measurements will be performed on a regular basis, which is essential for applying the system, for example, to continuously monitor the snowpack evolution in an avalanche start zone. Challenges for continuous recording in a remote area include energy issues. From an operational point of view, the system needs to be further developed in terms of automatic signal processing and data interpretation.

Acknowledgements

We acknowledge suggestions by anonymous reviewers that helped to improve the paper. The research project was completed within the framework of the D-A-CH consortium (DFG-FWF-SNF) with Deutsche Forschungsgemeinschaft (DFG) as lead agency. C.M. was funded by the Swiss National Science Foundation (SNF); A.H. was supported by DFG grant EI 672/6; and O.E. by the DFG Emmy Noether-programme grant EI 672/5. In addition we want to thank Hans-Martin Schuler from IGM (Ingenieurgesellschaft für Geophysikalische Messtechnik) for providing the radar control unit and PIEPS GmbH for incentive support.

References

Albert, M.R., Koh, G., Perron, F., 1999. Radar investigations of melt pathways in a natural snowpack. Hydrol. Process. 13, 2991–3000.
Arck, M., Scherer, D., 2002. Problems in the determination of sensible heat flux over snow. Geogr. Ann. 84 (3–4), 157–189.
Baggi, S., Schweizer, J., 2009. Characteristics of wet snow avalanche activity: 20 years of observations from a high alpine valley (Dischma, Switzerland). Nat. Hazard. 50 (1), 97–108.
Bartelt, P., Lehning, M., 2002. A physical SNOWPACK model for the Swiss avalanche warning; part I: numerical model. Cold Reg. Sci. Technol. 35 (3), 123–145.
Bellaire, S., Pielmeier, C., Schneebeli, M., Schweizer, J., 2009. Stability algorithm for snow micro-penetrometer measurements. J. Glaciol. 55 (193), 805–813.
Bhutiyani, M.R., 1994. Field investigations on melt water percolation and its effect on shear strength of wet snow. In: Agrawal, K.C. (Ed.), Proceedings Snow Symp-94. Snow and Avalanche Study Establishment. Manali (H.P.), India, pp. 200–206.
Boyne, H.S., Fisk, D.J., 1990. A laboratory comparison of field techniques for measurements of the liquid water fraction of snow. CRREL Special Report 90-3. 12 pp.
Bradford, J., Harper, J., Brown, J., 2009. Complex dielectric permittivity measurements from ground-penetrating radar data to estimate snow liquid water content in the pendular regime. Water Resour. Res. 45, W08403. doi:10.1029/2008WR007341.
Colbeck, S.C., 1972. A theory of water percolation in snow. J. Glaciol. 11 (63), 369–385.
Daniels, D., 2004. Ground Penetrating Radar. The Institution of Electrical Engineers, London, UK.
Denoth, A., 1980. The pendular–funicular liquid transition in snow. J. Glaciol. 25 (91), 93–97.
Denoth, A., 1989. Snow dielectric measurements. Adv. Space Res. 9 (1), 233–243.
Denoth, A., 1994. An electronic device for long-term snow wetness recording. Ann. Glaciol. 19, 104–106.
Denoth, A., Foglar, A., Weiland, P., Mätzler, C., Aebischer, H., Tiuri, M., Sihvola, A., 1984. A comparative study of instruments for measuring the liquid water content of snow. J. Appl. Phys. 56 (7), 2154–2160.
Egli, L., Jonas, T., Meister, R., 2009. Comparison of different automatic methods for estimating snow water equivalent. Cold Reg. Sci. Technol. 57 (2–3), 107–115.
Fierz, C., Föhn, P.M.B., 1995. Long-term observation of the water content of an alpine snowpack. Proceedings International Snow Science Workshop, Snowbird, Utah, U.S.A., 30 October-3 November 1994. ISSW 1994 Organizing Committee, Snowbird UT, USA, pp. 117–131.
Fierz, C., Armstrong, R.L., Durand, Y., Etchevers, P., Greene, E., McClung, D.M., Nishimura, K., Satyawali, P.K., Sokratov, S.A., 2009. The International Classification for Seasonal Snow on the Ground. 83 HP-VII Technical Documents in Hydrology. UNESCO-IHP, Paris, France. 90 pp.
Föhn, P.M.B., 1987. The Rutschblock as a practical tool for slope stability evaluation. In: Salm, B., Gubler, H. (Eds.), Symposium at Davos 1986—Avalanche Formation, Movement and Effects, IAHS Publ., 162. International Association of Hydrological Sciences, Wallingford, Oxfordshire, U.K., pp. 223–228.
Harper, J., Bradford, J., 2003. Snow stratigraphy over a uniform depositional surface: spatial variability and measurement tools. Cold Reg. Sci. Technol. 37 (3), 289–298.
Heilig, A., Schneebeli, M., Fellin, W., 2008. Feasibility study of a system for airborne detection of avalanche victims with ground penetrating radar and a possible automatic location algorithm. Cold Reg. Sci. Technol. 51 (2–3), 178–190.
Heilig, A., Schneebeli, M., Eisen, O., 2009. Upward-looking ground-penetrating radar for monitoring snowpack stratigraphy. Cold Reg. Sci. Technol. 59 (2–3), 152–162.
Heilig, A., Eisen, O., Schneebeli, M., 2010. Temporal observations of a seasonal snowpack using upward-looking GPR. Hydrol. Process. 24 (22), 3133–3145.
Hirashima, H., Yamaguchi, S., Sato, A., Lehning, M., 2010. Numerical modelling of liquid water movement through layered snow based on new measurements of the water retention curve. Cold Reg. Sci. Technol. 64 (2), 94–103.
Instanes, A., Lonne, I., Sandaker, K., 2004. Location of avalanche victims with ground-penetrating radar. Cold Reg. Sci. Technol. 38 (1), 55–61.
Kawashima, K., Endo, T., et al., 1998. A portable calorimeter for measuring liquid-water content of wet snow. Ann. Glaciol. 26, 103–106.
Lehning, M., Bartelt, P., Brown, R.L., Fierz, C., Satyawali, P.K., 2002a. A physical SNOWPACK model for the Swiss avalanche warning; part II. Snow microstructure. Cold Reg. Sci. Technol. 35 (3), 147–167.
Lehning, M., Bartelt, P., Brown, R.L., Fierz, C., 2002b. A physical SNOWPACK model for the Swiss avalanche warning; part III: meteorological forcing, thin layer formation and evaluation. Cold Reg. Sci. Technol. 35 (3), 169–184.
Lundberg, A., 1997. Laboratory calibration of TDR-probes for snow wetness measurements. Cold Reg. Sci. Technol. 25 (3), 197–205.
Lundberg, A., Thunehed, H., 2000. Snow wetness influence on impulse radar snow surveys theoretical and laboratory study. Nord. Hydrol. 31 (2), 89–106.
Lundberg, A., Thunehed, H., Bergström, J., 1999. Impulse radar snow surveys—influence of snow density. Nord. Hydrol. 31 (1), 1–14.
Machado, A., 2000. Spatial and temporal variability of meltwater pathways in a continental subalpine snowpack. M.Sc. thesis, University of Colorado, Boulder, Colorado, USA.
Machguth, H., Eisen, O., Paul, F., Hoelzle, M., 2006. Strong spatial variability of snow accumulation observed with helicopter-borne GPR on two adjacent Alpine glaciers. Geophys. Res. Lett. 33 (13), L13503.
Marchand, W.-D., Bruland, O., Killingtveit, A., 2001. Improved measurements and analysis of spatial snow cover by combining a ground based radar system with a differential global positioning system receiver. Nord. Hydrol. 32 (3), 181–194.
Marshall, H.-P., Koh, G., 2008. FMCW radars for snow research. Cold Reg. Sci. Technol. 52 (2), 118–131.
Matzl, M., Schneebeli, M., 2006. Measuring specific surface area of snow by near infrared photography. J. Glaciol. 42 (179), 558–564.
McClung, D.M., Schaerer, P., 2006. The Avalanche Handbook. The Mountaineers Books, Seattle WA, U.S.A.
Mitterer, C., Mott, R., Schweizer, J., 2009. Observations and analysis of two wet-snow avalanche cycles. In: Schweizer, J., van Herwijnen, A. (Eds.), International Snow Science Workshop ISSW, Davos, Switzerland, 27 September–2 October 2009. Swiss Federal Institute for Forest, Snow and Landscape Research WSL, pp. 262–266.
Mitterer, C., Hirashima, H., Schweizer, J., 2011. Wet-snow instabilities: comparison of measured and modelled liquid water content and snow stratigraphy. Ann. Glaciol. 52 (58).
Modroo, J., Olhoeft, G.R., 2004. Ground penetrating radar location of buried avalanche victims. In: Elder, K. (Ed.), Proceedings ISSW 2004. International Snow Science Workshop, Jackson Hole WY, U.S.A., pp. 399–408. 19–24 September 2004.
Mualem, Y., 1976. New model for predicting hydraulic conductivity of unsaturated porous-media. Water Resour. Res. 12 (3), 513–522.
Perla, R., 1991. Real permittivity of snow at 1 MHz and 0 °C. Cold Reg. Sci. Technol. 19 (2), 215–219.
Romig, J.M., Custer, S.G., Birkeland, K.W., Locke, W.W., 2005. March wet avalanche prediction at Bridger Bowl Ski Area, Montana. In: Elder, K. (Ed.), Proceedings ISSW 2004. International Snow Science Workshop, Jackson Hole WY, U.S.A., pp. 598–607. 19–24 September 2004.
Roth, K., Schulin, R., Flühler, H., Attinger, W., 1990. Calibration of time domain reflectometry for water-content measurement using a composite dielectric approach. Water Resour. Res. 26 (10), 2267–2273.
Schneebeli, M., 1995. Development and stability of preferential flow paths in a layered snowpack. In: Tonnessen, K.A., Williams, M.W., Tranter, M. (Eds.), Biogeochemistry of Seasonally Snow-Covered Catchments (Proceedings of Symposium at Boulder (CO), U.S.A., July 1995). : IAHS Publication, 228. International Association of Hydrological Sciences, Wallingford, Oxfordshire, U.K., pp. 89–95.
Schneebeli, M., Johnson, J.B., 1998. A constant-speed penetrometer for high-resolution snow stratigraphy. Ann. Glaciol. 26, 107–111.
Schweizer, J., Jamieson, J.B., 2007. A threshold sum approach to stability evaluation of manual snow profiles. Cold Reg. Sci. Technol. 47 (1–2), 50–59.
Schweizer, J., Jamieson, J.B., Schneebeli, M., 2003. Snow avalanche formation. Rev. Geophys. 41 (4), 1016.
Sihvola, A.H., Kong, J.A., 1988. Effective permittivity of dielectric mixtures. IEEE T. Geosci. Remote 26 (4), 420–429.
Sihvola, A., Tiuri, M., 1986. Snow fork for field determination of the density and wetness profiles of a snow pack. IEEE T. Geosci. Remote 24 (5), 717–721.
Stähli, M., Stacheder, M., Gustafsson, D., Schlaeger, S., Schneebeli, M., Brandelik, A., 2004. A new in situ sensor for large-scale snow-cover monitoring. Ann. Glaciol. 38, 273–278.
Techel, F., Pielmeier, C., 2010. Snowpack properties of unstable wet snow slopes: observations from the Swiss Alps. Proceedings International Snow Science Workshop ISSW, Lake Tahoe CA, U.S.A., 17–22 October 2010, p. 197-193.
Techel, F., Pielmeier, C., 2011. Point observations of liquid water content in wet snow—investigating methodical, spatial and temporal aspects. Cryosphere 5, 405–418.
Topp, G.C., Davis, J.L., Annan, A.P., 1980. Electromagnetic determination of soil water content: measurements in coaxial transmission lines. Water Resour. Res. 16 (3), 574–582.

Trautman, S., 2008. Investigations into wet snow. Avalanche Rev. 26 (4), 16–17 21.
van Genuchten, M.T.A., 1980. A closed-form equation for predicting the hydraulic conductivity of unsaturated flow. Soil Sci. Soc. Am. J. 44, 892–898.
Waldner, P.A., Schneebeli, M., Schultze-Zimmerman, U., Flühler, H., 2004. Effect of snow structure on water flow and solute transport. Hydrol. Process. 18 (7), 1271–1290.
Wilhelms, F., 2005. Explaining the dielectric properties of firn as a density-and-conductivity mixed permittivity (DECOMP). Geophys. Res. Lett. 32 (16), L16501.
Yamaguchi, S., Katsushima, T., Sato, A., Kumakura, T., 2010. Water retention curve of snow with different grain sizes. Cold Reg. Sci. Technol. 64 (2), 87–93.